XII International Conference on Computational Plasticity. Fundamentals and Applications
COMPLAS XII
E. Oñate, D.R.J. Owen, D. Peric and B. Suárez (Eds)

CONSTRUCTION OF 3D STATISTICALLY SIMILAR RVES FOR DUAL-PHASE STEEL MICROSTRUCTURES

Daniel Balzani, Lisa Scheunemann, Dominik Brands and Jörg Schröder

Institute of Mechanics, Faculty of Engineering
University Duisburg-Essen
Universitätsstr. 15, 45141 Essen, Germany
e-mail: daniel.balzani@uni-due.de, web page: http://www.uni-due.de/mechanika

Key words: FE^2 method, homogenization, statistically similar RVE, finite plasticity

Abstract. A method for the construction of 3D Statistically Similar RVEs for dual-phase steel (DP steel) microstructures in presented in this paper. DP steels have enhanced material properties compared to conventional steels which make them favorable for many engineering applications. Since these properties originate from the microstructure of the two-phase material, microstructural effects should be taken into account. This can be achieved by using the FE^2 method, however, this method requires RVEs of low complexity in order to end up in calculations with reasonable computing time. Instead of using RVEs as direct substructures of a real microstructure, SSRVEs with less complex inclusion morphology can be constructed, which still represent the mechanical response of the material accurately enough while providing a speedup due to the lower complexity of discretization. The method for the construction of such SSRVEs described here is based on the minimization of a least-square functional taking into account distinct statistical measures computed for the real microstructure and the SSRVE. Here, the focus is on the construction of three-dimensional SSRVEs. The performance of those SSRVEs is shown and an inhomogeneous numerical example using the FE^2 method combined with SSRVEs is presented.

1 INTRODUCTION

Advanced high strength steels, as e.g. dual-phase steels, affect many fields of today's engineering applications. The material properties have significantly improved compared to conventional steels and offer higher strength and formability finding a broad variety of applications in the fields of mobility, manufacturing and safety. The improved material properties originate from the interaction of the constituents of the material at the microscale, a soft ferrite matrix with hard martensite inclusions, cf. [7]. This raises the idea of a direct incorporation of the microstructure into the computation to consider this phenomenon. The FE^2 method, see eg. [4] and [10], is an appropriate tool for this purpose. There, a microscopic boundary value problem which is governed by the FE discretization

of a representative volume element (RVE) reflecting the real microstructure is solved at each macroscopic Gauss point. However, due to the underlying morphology of a real microstructure, the discretization of such a RVE is typically complex. The large number of degrees of freedom (dof) required for the discretization of those classical RVEs makes the method computationally inefficient for many applications. The construction of RVEs with a lower complexity can circumvent this issue. These RVEs should be more simple in their morphology while they are still able to represent the mechanical behavior of the real microstructure. Statistically similar RVEs (SSRVEs) have shown to serve well as such structures in the two-dimensional case, see e.g. [11]. They are characterized by similarities compared to the real microstructure with respect to statistical measures describing the microstructure morphology and to the mechanical behavior. For the construction, a least-square functional is minimized considering certain statistical measures computed for the real microstructure and the SSRVE. A well-posed SSRVE can be assumed for a low error in the least-square functional. As descriptors for the inclusion morphology, basic scalar-valued parameters, such as the volume fraction, see e.g. [5], as well as higher order measures such as the lineal-path function or spectral density, have proven their applicability in this method. However, they contribute to the well-posedness of the SSRVE differently, for more details see [1].
Here we focus on the construction of three-dimensional SSRVEs for a DP steel microstructure. The performance of the constructed SSRVEs is evaluated by comparing their mechanical response with the real microstructure . In addition, substructures of the entire microstructure, also identified based on the statistical measures, are investigated and compared with the aforementioned SSRVEs that are constructed using an artificial microstructure morphology. In a numerical example addressing the Nakajima test, the applicability of 3D SSRVEs in inhomogeneous boundary value problems is shown.

2 METHOD FOR THE CONSTRUCTION OF SSRVES

For the construction of SSRVEs we assume that the real (not necessarily periodic) microstructure can be represented by a periodic microstructure, see Fig. 1. Then only the periodic unitcell has to be considered in calculations provided that periodic boundary conditions are applied. Such a periodic unitcell is regarded as statistically similar RVE (SSRVE). These structures are governed by a less complex inclusion morphology which is considered as statistically similar with regard to certain statistical measures, but which still represent the mechanical response of the real microstructure. For the construction of SSRVEs in 2D, a method is proposed in [11] and is extended to 3D here. For that purpose, a least square functional comparing the statistical measures for the real microstructure and the SSRVE is minimized, i.e. a suitable parameterization of the SSRVE's microstructure is given by

$$\boldsymbol{\gamma}^* := \operatorname{argmin}\left[\mathcal{L}\left(\boldsymbol{\gamma}\right)\right] \qquad \text{with} \qquad \mathcal{L}(\boldsymbol{\gamma}) \;:=\; \sum_{i=1}^{\text{nsm}} \omega_i \;\left(\mathcal{P}_i^{\text{real}} - \mathcal{P}_i^{\text{SSRVE}}\left(\boldsymbol{\gamma}\right)\right)^2 . \tag{1}$$

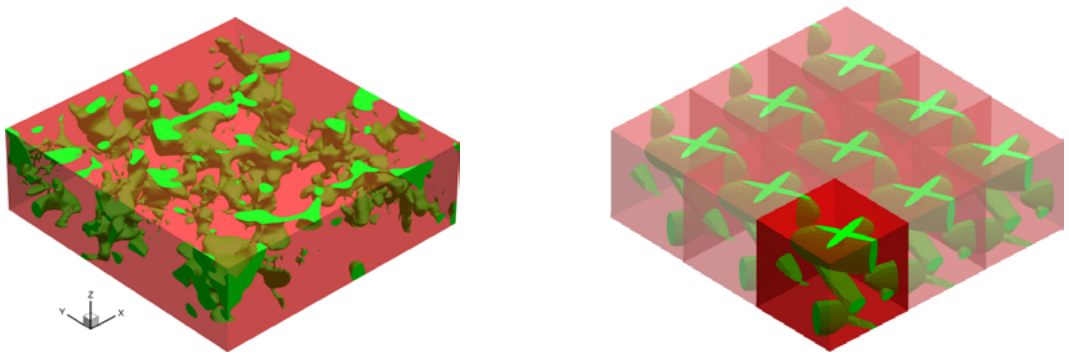

(a) (b)

Figure 1: Schematic illustration of the basic concept, red indicating the matrix phase, green indicating the inclusion phase: (a) usual RVE with arbitrary inclusion morphology and (b) periodic microstructure with SSRVE as unitcell.

$\mathcal{P}^{\text{real}}$ and $\mathcal{P}^{\text{SSRVE}}$ represent appropriate statistical measures of the real microstructure and the SSRVE, respectively, with the total number of statistical measures considered as nsm, the individual weighting factors ω and the vector $\boldsymbol{\gamma}$ describing the inclusion morphology of the SSRVE.

2.1 Statistical measures

An overview on statistical measures to describe the morphology of a single phase in a multiphase material can be e.g. found in [5]. Rather general but yet important information is contained in some scalar-valued basic parameters, the volume fraction (V), the specific internal surface (S) and the specific integral of mean curvature (M) which are defined as

$$\mathcal{P}_V = \frac{V_I}{V}, \qquad \mathcal{P}_S = \frac{S_I}{V} \qquad \text{and} \qquad \mathcal{P}_M = \frac{1}{2V}\int_S \left(\min_\beta [\kappa] + \max_\beta [\kappa]\right) ds, \tag{2}$$

with V_I and V denoting the volume of the inclusion phase and total volume, respectively. S_I is the interface area of the inclusion phase, $\kappa := \kappa(\beta)$ denotes the curvature varying with β in the tangential plane. As it was found in [1] these parameters alone are not sufficient to characterize random microstructures and thus statistical measures of higher order are considered. The spectral density is computed based on the discrete Fourier transformation of the microstructure multiplied with its conjugate complex:

$$\mathcal{P}_{SD}(n_x, n_y, n_z) := \frac{1}{2\pi N_x N_y N_z} \left|\mathcal{F}(n_x, n_y, n_z)\right|^2 \tag{3}$$

with the discrete Fourier transformation given by

$$\mathcal{F}(n_x, n_y, n_z) := \sum_{k_x=1}^{N_x}\sum_{k_y=1}^{N_y}\sum_{k_z=1}^{N_z} \exp\left(2\pi \mathrm{i}\left(\frac{n_x\, k_x}{N_x}\frac{n_y\, k_y}{N_y}\frac{n_z\, k_z}{N_z}\right)\right) \chi\left(k_x, k_y, k_z\right). \tag{4}$$

Here, n_x, n_y and n_z are the coordinates of the frequency domain, N_x, N_y and N_z are the numbers of voxels in the binary data set representing the microstructure and k_x, k_y and k_z define the position in this binary set. The indicator function χ is given by

$$\chi\left(k_x, k_y, k_z\right) := \begin{cases} 1 & \text{if point } x\left(k_x, k_y, k_z\right) \text{ lies in inclusion phase,} \\ 0 & \text{otherwise.} \end{cases} \tag{5}$$

Due to the fact that the spectral density captures periodicity effects in a microstructure, it plays a key role for finding a simplified periodic microstructure. In addition, this statistical measure is strongly correlated to the two-point probability function, see [6]. Another statistical measure considered here is the lineal-path function. It represents the probability of a line segment of a distinct length and orientation being located completely in one phase, here the inclusion phase. Complete lineal-path functions computed for all possible lengths and orientations result in massive computational costs, hence, the lineal-path function is computed for a certain number of line segments only, which are regularly distributed. As for the spectral density, an indicator function for the lineal-path function is defined by

$$\lambda(p+m, q+k, o+l) := \begin{cases} 1 & \text{if line segment } \overrightarrow{\mathbf{x_1 x_2}} \text{ is in inclusion phase,} \\ 0 & \text{otherwise,} \end{cases} \tag{6}$$

with the line segment $\overrightarrow{\mathbf{x_1 x_2}}$ defined by the start point $\mathbf{x}_1(p, q, o)$ and the end point $\mathbf{x}_2(m, k, l)$ as points in the binary data set representing the microstructure. The lineal path function is then computed by

$$\mathcal{P}_{LP}(m, k, l) := \frac{1}{N_x N_y N_z} \sum_{p=1}^{N_x} \sum_{q=1}^{N_y} \sum_{o=1}^{N_z} \lambda(p+m, q+k, o+l). \tag{7}$$

2.2 Proposed method

Focusing on the phase fraction, the spectral density and the lineal-path function the explicit least square functional is given by

$$\begin{aligned} \mathcal{L}(\boldsymbol{\gamma}) \;&:=\; \omega_V \left(\mathcal{P}_V^{\text{real}} - \mathcal{P}_V^{\text{SSRVE}}\left(\boldsymbol{\gamma}\right)\right)^2 \\ &+\; \omega_{SD} \sum_{k_x, k_y, k_z} \left(\mathcal{P}_{SD}^{\text{real}} - \mathcal{P}_{SD}^{\text{SSRVE}}\left(\boldsymbol{\gamma}\right)\right)^2 \\ &+\; \omega_{LP} \sum_{p,q,o} \left(\mathcal{P}_{LP}^{\text{real}} - \mathcal{P}_{LP}^{\text{SSRVE}}\left(\boldsymbol{\gamma}\right)\right)^2 \end{aligned} \tag{8}$$

with the weighting factors $\omega_V = 1$, $\omega_{SD} = 1$ and $\omega_{LP} = 1000$, which were found to give reasonable results. For the solution of the optimization problem the differential evolution

optimizer in the "mystic"-framework (http://dev.danse.us/trac/mystic) is applied. Note that the inclusion geometry is technically constructed such that periodic extensibility of the SSRVE can be provided. As an example analysis the real microstructure of a DP steel is considered as a target random microstructure. This microstructure is obtained by 3D Electron Backscatter Diffraction (EBSD) combined with Focused Ion Beam (FIB). The measurements were carried out at Max Planck Institut für Eisenforschung, Prof. D. Raabe, Düsseldorf, for details on the method see e.g. [8] and [14]. The real microstructure was measured with a size of 16.45 µm x 15.9 µm x 5.0 µm and discretized for FE computations with 10-noded tetrahedral elements containing 8.5 mio dof.

2.3 SSRVEs based on substructuring

The most natural method to define a RVE for a real microstructure is choosing the smallest possible substructure which still represents the mechanical response of the whole microstructure precisely. Starting from this idea, a SSRVE given as a substructure of the real microstructure is determined by comparing all possible substructures of a certain size with the complete microstructure regarding distinct statistical measures. Here, the phase fraction, the internal surface density, the integral of mean curvature, the spectral density and the lineal-path function are considered. The substructure having the lowest error in the statistical measure can be considered as the best choice of a SSRVE based on substructuring for the entire microstructure. For a real microstructure, cubic SSRVEs based on substructuring were computed for side lengths $a = 1.25\mu m$, $2.5\mu m$ and $5.0\mu m$. The obtained substructures are shown in Fig. 2. Table 1 summarizes the results of the statistical measures for the three generated substructures. Not surprisingly, the lowest error in statistical measures can be found in the largest SSRVE, however it also requires the largest number of elements for the discretization.

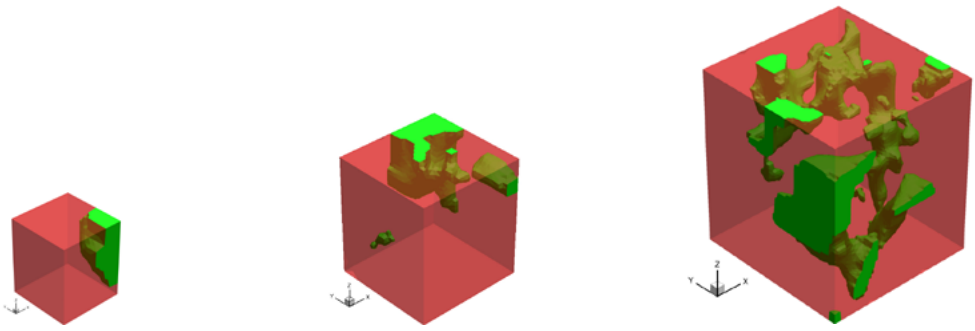

(a) (b) (c)

Figure 2: Construction of SSRVE based on substructuring: (a) SSRVE substructure with $a = 1.25\mu m$, (b) SSRVE substructure with $a = 2.5\mu m$ (scaled view) and (c) SSRVE substructure with $a = 5.0\mu m$ (scaled view)

Table 1: Error of statistical measures for SSRVEs based on substructuring

SSRVE	$\mathcal{L}$ $[10^{-2}]$	$\mathcal{L}_V$ $[10^{-4}]$	$\mathcal{L}_{surf}$ $[10^{-3}]$	$\mathcal{L}_{curv}$ $[10^{-3}]$	$\mathcal{L}_{SD}$ $[10^{-3}]$	$\mathcal{L}_{LP}$ $[10^{-4}]$	n_{ele}
ω	-	1	1	1	1	1000	-
$a = 1.25\mu m$	12.83	77.0	1.9	6.0	12.0	1.0	5 695
$a = 2.5\mu m$	2.33	3.0	0.36	0.1	4.6	0.2	42 279
$a = 5.0\mu m$	0.78	1.3	1.2	2.4	1.7	0.024	707 676

2.4 SSRVEs based on artificial morphology

Another approach for the construction of SSRVEs is to assume a simplified inclusion morphology for the structures. Here, the inclusion morphology is assumed to be built up by different numbers of non rotationally symmetric ellipsoids. One ellipsoid can be described by a set of nine parameters, which enter the parameterization vector for one ellipsoid in the minimization problem: $\boldsymbol{\gamma} = [x_c\ y_c\ z_c\ \psi\ \theta\ \phi\ r_1\ r_2\ r_3]$. In this formulation, x_c, y_c and z_c describe the center point of the ellipsoid, ψ, θ and ϕ measure the rotation of the coordinate system of the ellipsoid and r_1, r_2 and r_3 define the radii on the semi axis of the ellipsoid. For a number of n_{inc} ellipsoids in a SSRVE, the parameterization vector consists of n_{inc} times the parameters for each ellipsoid. The number of inclusions is also important for the determination of the size of the SSRVE. Since the lineal-path function somehow depends on length dimension, it may conflict with the measure of phase fraction, if the size of the SSRVE is not chosen large enough. In this case, during the minimization process, the size of an average ellipsoidal inclusion in the real microstructure would be larger than the volume fraction admits. To avoid this, the size of an average ellipsoidal inclusion is calculated from the lineal path function of the real microstructure with a threshold of 2% probability. For this average ellipsoid, the volume V_{aver} can be calculated based on measurements of the semi axis. Then, the size of a cubic SSRVE with

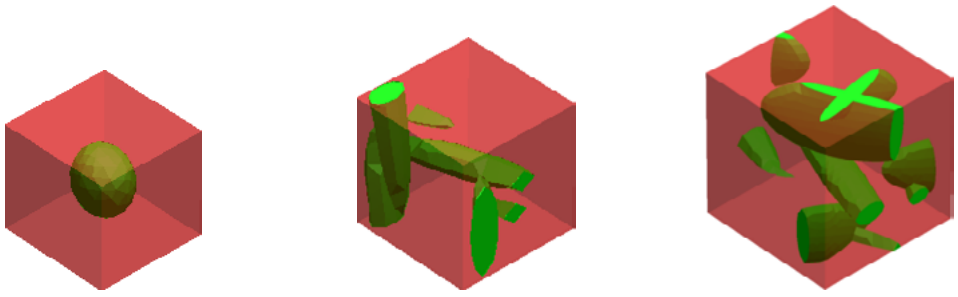

(a) (b) (c)

Figure 3: SSRVE with ellipsoidal inclusions: (a) $n_{\text{inc}} = 1$ $[l_x = 3.0\mu m]$, (b) $n_{\text{inc}} = 2$ $[l_x = 3.8\mu m]$ and (c) $n_{\text{inc}} = 3$ $[l_x = 4.3\mu m]$.

Table 2: Error in statistical measures of artificial SSRVEs.

SSRVE	$\mathcal{L}[10^{-2}]$	$\mathcal{L}_V[10^{-4}]$	$\mathcal{L}_{SD}[10^{-3}]$	$\mathcal{L}_{LP}[10^{-4}]$	n_{ele}
$n_{\text{inc}} = 1$	8.432	485.29	4.5	0.31	2851
$n_{\text{inc}} = 2$	0.98	32.07	3.5	0.031	5015
$n_{\text{inc}} = 3$	0.53	3.37	3.3	0.017	18835

$l_x = l_y = l_z$ can be estimated depending on the number of ellipsoidal inclusions n_{inc} by

$$\mathcal{P}_{\text{V}}^{\text{real}} = \frac{n_{\text{inc}}\, V_{\text{aver}}}{V^{\text{SSRVE}}}, \tag{9}$$

$$\rightarrow l_x = l_y = l_z = \sqrt[3]{V^{\text{SSRVE}}} = \frac{n_{\text{inc}}\, V_{\text{aver}}}{\mathcal{P}_{\text{V}}^{\text{real}}}. \tag{10}$$

SSRVEs with one, two and three ellipsoidal inclusions are constructed to analyze the performance of the method and compared to the SSRVEs based on substructuring in section 2.3. The parallel optimization environment Mystic, cf. [3], is used for the minimization process. Fig. 3 shows the resulting SSRVEs, the errors of the statistical measures are summarized in table 2. In [1] it was found that the influence of the specific internal surface and the specific integral of mean curvature is negligible for such artificial SSRVEs in 2D, hence these measures are not considered here. As the complexity of inclusion morphology is increased, the error in the statistical measures decreases. Again, due to the higher complexity, the number of elements for the discretization also increases.

3 COMPARATIVE STUDY FOR MECHANICAL RESPONSE

An analysis of the performance of the different SSRVEs is carried out by comparing the mechanical response with the one of the real target microstructure. Two virtual experiments are carried out, tension in x-direction $[x]$ and shear of xz-plane in x-direction $[xy]$. For comparative purposes, a relative error measure is defined for each virtual experiment as

$$\tilde{r}_j := \sqrt{\frac{1}{n}\sum_{i=1}^{n}\left[r_j^{(i)}\right]^2} \qquad \text{with} \qquad r_j^{(i)} := \frac{\bar{\sigma}_{j,i}^{\text{real}} - \bar{\sigma}_{j,i}^{\text{SSRVE}}}{\bar{\sigma}_{j,i}^{\text{real}}}, \tag{11}$$

with j indicating the virtual experiment, i and n describing the individual and total number of evaluation points and $\bar{\sigma}$ defining the homogenized macroscopic stress. As an overall average error for each SSRVE,

$$\tilde{r} := \sqrt{\frac{1}{2}(\tilde{r}_x^2 + \tilde{r}_{xy}^2)} \tag{12}$$

is defined. The mechanical error is depicted in Fig. 4, table 3 summarizes the average mechanical errors. Note that a classical J_2 finite plasticity model with isotropic exponential hardening is used with parameters chosen such that the characteristic behavior of the

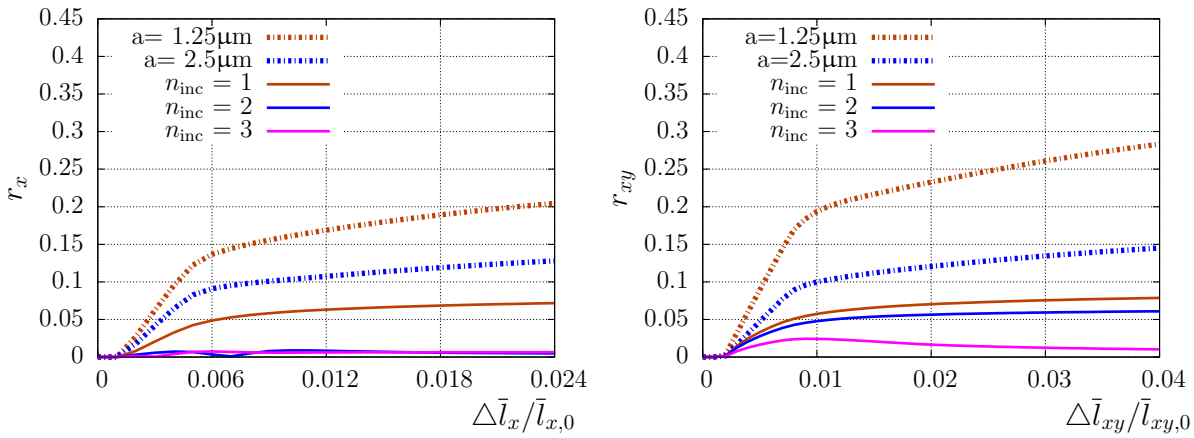

(a) (b)

Figure 4: Error of mechanical response of SSRVEs based on substructuring and artificial SSRVEs in virtual experiments: (a) tension test $[x]$ and (b) shear test $[xy]$.

single microscopic constituents in DP steel is represented reasonably. The substructuring SSRVE with $a = 5\mu\text{m}$ leads to a rather large number of finite elements (707 676) required for discretization and thus, this RVE can not be interpreted as a suitable SSRVE since the gain in computational efficiency will be rather small. Thus, the analysis was not carried out for this SSRVE.

Comparing the two SSRVEs based on substructures with each other, a lower mechanical error compared to the real microstructure was found for the larger one in both virtual experiments. This appears to be natural, because a larger size can capture more parts of the morphology. Due to the large inclusions in the real microstructure, both these SSRVEs are mainly governed by one large inclusion. Furthermore, the structure of the SSRVEs taken from a real microstructure does not provide periodic morphology properties, thus linear displacement boundary conditions are applied in this case. The application of these boundary conditions are known to be too stiff if the inclusion with higher stiffness is located at the boundary of the RVE. This may also influence the resulting error. This effect

Table 3: Error in % of mechanical response of SSRVEs based on substructuring and artificial SSRVEs.

SSRVE	$\tilde{r}_x$	$\tilde{r}_{xy}$	$\tilde{r}$
$a = 1.25\,\mu\text{m}$	14.6 ± 6.1	20.5 ± 8.1	17.80
$a = 2.5\,\mu\text{m}$	9.4 ± 3.8	10.6 ± 4.2	10.02
$n_{\text{inc}} = 1$	5.3 ± 2.2	5.5 ± 2.2	5.40
$n_{\text{inc}} = 2$	0.55 ± 0.24	4.4 ± 1.7	3.13
$n_{\text{inc}} = 3$	0.53 ± 0.22	1.5 ± 0.6	1.12

has obviously more influence in smaller structures, where the boundary effect becomes more prominent. It can be noticed that the results of the mechanical error behave proportionally compared to the behavior of the statistical error, see table 1. A lower error in the statistical measures is related to a lower error in the mechanical response.
The SSRVEs with artificial morphology show a lower mechanical error when the number of inclusions n_{inc} and thereby somehow the complexity is increased. For the tension test, both SSRVEs with one and two inclusions show a similar error. As before, the behavior of the statistical error is proportional to the mechanical error, giving the best overall result for the SSRVE with the most complex inclusion morphology. Comparing the performance of the different types of SSRVEs, the SSRVEs based on artificial inclusion morphology clearly show a better approximation behavior of the real microstructure. Even the simplest SSRVE with 1 ellipsoidal inclusion achieves a lower error, 5.4% than the complex SSRVE taken as a substructure with $a = 2.5\mu\text{m}$ with 10%. Taking a closer look at the computational effort, the substructures also need a higher number of elements than the artificial SSRVEs. Note that an automated mesh generator with the same parameters is used for the discretization of all SSRVEs. Even though the best SSRVE from substructures requires more than twice as many elements than the best SSRVE with artificial morphology its mechanical error is almost ten times higher. Thus, it can be concluded that artificial SSRVEs may be favorable.

4 NUMERICAL EXAMPLE: NAKAJIMA TEST

The high computational cost of the FE^2 method based on the classical choice of RVEs is one of the main obstacles using it for the simulation of a variety of applications such as forming processes. Using SSRVEs instead the computational effort reduces significantly such that full three-dimensional multiscale simulations are enabled. As an application example we choose the Nakajima test, which is a challenging boundary value problem in the field of sheet metal forming simulations. It has become a standard experimental method for the determination of forming limit diagrams (FLD) and is standardized by the ISO/DIS 12004-2, see [2]. During the experiments a hemispherical punch is driven into a clamped sheet metal until failure arises. The usage of different sheet geometries specified in the aforementioned ISO standard cause different stress-strain conditions at the location where failure initiates: from almost uniaxial up to biaxial tension conditions. Here, we consider a sheet geometry with a blank width of 20 mm in the middle of the sheet. For the numerical simulation we only consider a quarter of the whole blank as macroscopic boundary value problem and apply reasonable symmetry conditions. Note that for the results shown below we expand symmetrically the macroscopic geometry to the full one. The clamping of the sheet metal at both ends is idealized by displacement boundary conditions. The punch is approximated by a simple penalty contact formulation and is driven orthogonally into the sheet surface. Additionally, we reduce the computational cost by applying the FE^2 approach only to a part of special interest where failure is expected to arise –the FE^2-region. For that reason we define a circular area, cf. Figure 5,

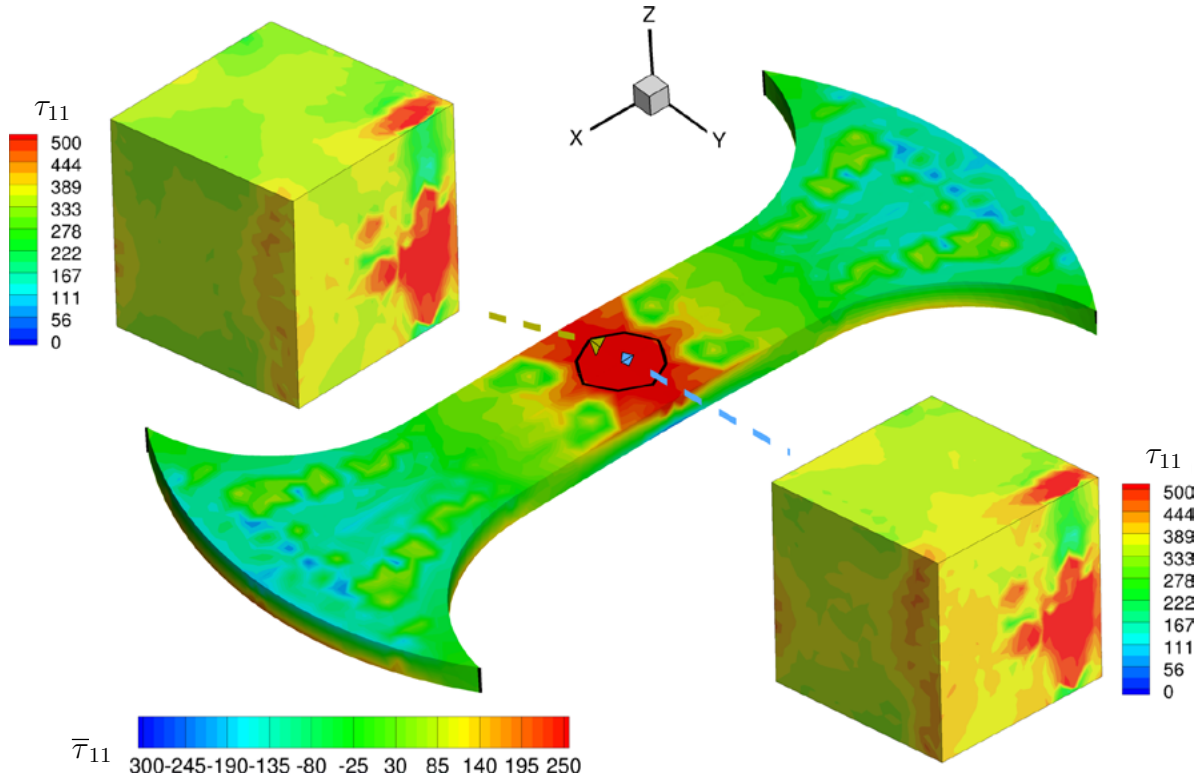

Figure 5: Distribution of the Kirchhoff stresses $\overline{\tau}_{11}$ and τ_{11} ("1" indicates the x-direction), respectively, in the macroscopic and two selected microscopic boundary value problems at a punch displacement $u = 1.5\,\text{mm}$. The FE^2-region is marked by a black line in the middle of the blank.

in the middle of the blank. For the rest of the blank a classical macroscopic J2-plasticity model using a von Mises type hardening law is used, the same one that is also used at the microscale of the FE^2 calculations, for details see e.g. [12]. The yield criterion uses the conjugated internal variable α and reads

$$\beta = 436\,\text{MPa} + 7\,\text{MPa}\,\alpha + (230\,\text{MPa} - 436\,\text{MPa})\,\exp(-16.7\alpha). \tag{13}$$

The material parameters are adjusted such that the mechanical behavior matches the virtual uniaxial tension and shear test that results from the target microstructure. Finally, we end up with 2145 tetrahedral finite elements using quadratic shape functions in the macroscopic discretization, whereof 94 elements are located in the FE^2-region. In the following example we apply the SSRVE with 2 ellipsoids to the microscopic boundary value problem. This represents a good compromise between accuracy and efficiency. Since each macroscopic element uses 5 integration points we have to solve 470 microscopic boundary value problems in each macroscopic iteration step. For an efficient computation we build an environment based on the finite element program FEAP by R.L. Taylor, see [13] with

a self-written FE^2-environment, which parallelizes the macroscopic assembling and thus the solution of the microscopic boundary value problems. The processor distribution is obtained via Message Passing Interface (MPI) to each computing node, where the PARDISO solver is used to solve the arising systems of equations, cf. [9]. Finally, the computation was performed on 20 computing nodes (24 cores each) of the supercomputer CRAY XT6m located at Duisburg-Essen University. The resulting stress response in the macroscopic and two selected microscopic boundary value problems are shown in Fig. 5 for a punch displacement of $u = 1.5\,\mathrm{mm}$. Comparing the maximal stress levels in the macroscopic and microscopic boundary value problems, a higher level is observed at the microscale, being an important issue with respect to the identification of failure initialization.

5 CONCLUSION

A method for the construction of 3D SSRVEs for real DP steel microstructures was proposed, which was based on distinct scalar and higher order statistical measures. In addition to SSRVEs constructed from substructures, SSRVEs with an artificial inclusion morphology were constructed based on the solution of a minimization problem. Both approaches showed that with an increase of complexity of the SSRVE morphology a lower error in the statistical measures was achieved. Additionally, more complex structures resulted in a decrease of the mechanical error. It was found that artificial SSRVEs allowed for a lower error in the statistical measures as well as in the mechanical response, at a lower number of finite elements required for discretization leading to FE^2 calculations of significantly increased efficiency. A numerical example showed the applicability of SSRVEs with artificial morphology.

Acknowledgement: Financial funding by the DFG-Research Group FOR 797-P8 project no. SCHR 570/8-2 is acknowledged. We appreciate Prof. D. Raabe (Max-Planck Institut für Eisenforschung, Düsseldorf) for providing the EBSD/FIB measurements. Furthermore, we thank the Center for Computational Sciences and Simulation (CCSS) of Duisburg-Essen University for their kind support regarding the calculations performed on the supercomputer Cray XT6m.

REFERENCES

[1] D. Balzani, D. Brands, J. Schröder, and C. Carstensen. Sensitivity analysis of statistical measures for the reconstruction of microstructures based on the minimization of generalized least-square functionals. *Technische Mechanik*, 30:297–315, 2010.

[2] ISO. Metallic materials -sheet and strip- determination of forming limit curves - part 2: Determination of forming limit curves in laboratory. ISO 12004–2:2008, International Organization for Standardization, Geneva, Switzerland, 2008.

[3] M.M. McKerns, L. Strand, T. Sullivan, A. Fang, and M.A.G. Aivazis. Building a framework for predictive science. *Proceedings of the 10th Python in Science Conference*, 2011.

[4] C. Miehe, J. Schröder, and C. G. Bayreuther. Computational homogenization analysis in finite plasticity. simulation of texture development in polycrystalline materials. *Computer Methods in Applied Mechanics and Engineering*, 171:387–418, 1999.

[5] J. Ohser and F. Mücklich. *Statistical analysis of microstructures in materials science*. J Wiley & Sons, 2000.

[6] E. Parzen. *Statistical processes*. Holden-Day, San Francisco, CA, 1992.

[7] N. Peranio, Y.J. Li, F. Roters, and D. Raabe. Microstructure and texture evolution in dual-phase steels: Competition between recovery, recrystallization and phase transformation. *Mater. Sc. Engin. A*, 527:4161–4168, 2010.

[8] D. Raabe S. Zaefferer, S.I. Wright. Three-dimensional orientation microscopy in a focused ion beam-scanning electron microscope: A new dimension of microstructure characterization. *Metal. Mater. Trans. A*, 39A:374–389, 2008.

[9] Olaf Schenk and Klaus Gärtner. Solving unsymmetric sparse systems of linear equations with PARDISO. *Future Generation Computer Systems*, 20(3):475 – 487, 2004.

[10] J. Schröder. *Homogenisierungsmethoden der nichtlinearen Kontinuumsmechanik unter Beachtung von Stabilitätsproblemen*. Habilitationsschrift, Bericht aus der Forschungsreihe des Instituts für Mechanik (Bauwesen), Lehrstuhl I, 2000.

[11] J. Schröder, D. Balzani, and D. Brands. Approximation of random microstructures by periodic statistically similar representative volume elements based on lineal-path functions. *Archive of Applied Mechanics*, 81:975–997, 2011.

[12] J.C. Simo. A framework for finite strain elastoplasticity based on maximum plastic dissipation and the multiplicative decomposition: Part i. continuum formulation. *Computer Methods in Applied Mechanics and Engineering*, 66:199–219, 1988.

[13] R. L. Taylor. FEAP - A Finite Element Analysis Program. Users manual, Structural Engineering, Mechanics and Materials, Department of Civil and Environmental Engineering, University of California, Berkeley, 2009. visited on 19. Mar. 2011.

[14] N. Zaafarani, D. Raabe, R. N. Singh, F. Roters, and S. Zaefferer. Three-dimensional investigation of the texture and microstructure below a nanoindent in a Cu single crystal using 3D EBSD and crystal plasticity finite element simulations. *Acta Materialia*, 54:1863–1876, 2006.